Supplemental Material for

Forced and natural dynamics of a clamped flexible fiber in wall turbulence

Giulio Foggi Rota, Morie Koseki, Riya Agrawal,* Stefano Olivieri,† and Marco Edoardo Rosti‡
Complex Fluids and Flows Unit, Okinawa Institute of Science and Technology Graduate University, 1919-1 Tancha, Onna-son, Okinawa 904-0495, Japan.

I. NUMERICAL METHODS

The motion of an incompressible fluid is governed by the incompressibility constraint and the momentum balance,

$$\nabla \cdot \mathbf{u} = 0, \tag{S1}$$

$$\frac{\partial \mathbf{u}}{\partial t} + \mathbf{u} \cdot \nabla \mathbf{u} = -\frac{1}{\rho_f} \nabla p + \nu \nabla^2 \mathbf{u} + \mathbf{f}_{\text{for}} + \mathbf{f}_{\text{fib}}, \tag{S2}$$

where $\mathbf{u}(\mathbf{x}, t)$ and $p(\mathbf{x}, t)$ denote the velocity and pressure fields, ρ_f is the volumetric density and ν the kinematic viscosity of the fluid. $\mathbf{f}_{\text{for}}$ and $\mathbf{f}_{\text{fib}}$ represent the forcing term needed to sustain a fully developed turbulent flow and that to account for the fluid-structure interaction, respectively [1]. The no-slip and no-penetration boundary conditions are enforced at the walls, while periodicity is imposed in the streamwise and spanwise directions. In this study, we tackle equations (S1,S2) numerically by means of the well tested solver *Fujin* (https://groups.oist.jp/cffu/code). The flow variables are sampled on a staggered Cartesian grid and all space derivatives are discretised with a second order central finite difference scheme; the solution is thus advanced in time with a second order Adams-Bashforth method [2]. We resort to a projection-correction algorithm [3], solving the Poisson equation for the pressure with an efficient decomposition library (*2decomp*) coupled to an in-place spectral solver based on the Fourier's series method described by Dorr [4].

Let us now consider a flexible fiber of length h and cross-section diameter d clamped at the wall, with homogeneous structural properties. Its dynamics is described by an extended version of the distributed-Lagrange-multiplier/fictitious-domain (DLM/FD) formulation of the continuum equations [5], which represents a generalisation of the Euler-Bernoulli beam model in that it allows for finite deflections, but retains the inextensibility constraint [6]:

$$\Delta\tilde{\rho} \frac{\partial^2 \mathbf{X}}{\partial t^2} = \frac{\partial}{\partial s}\left(T \frac{\partial \mathbf{X}}{\partial s}\right) - \gamma \frac{\partial^4 \mathbf{X}}{\partial s^4} - \mathbf{F} \tag{S3}$$

$$\frac{\partial \mathbf{X}}{\partial s} \cdot \frac{\partial \mathbf{X}}{\partial s} = 1 \tag{S4}$$

$\mathbf{X}(s, t)$ is the position of a point on the neutral axis of the fiber as a function of the curvilinear abscissa, s, and time, t, $\Delta\tilde{\rho} = (\rho_s - \rho_f)\pi d^2/4$ represents the difference among the linear density of the fiber and that of the fluid, T is the tension needed to enforce inextensibility, γ is the bending rigidity of the fiber and $\mathbf{F}$ is the fluid-structure coupling term. We impose $\mathbf{X}|_{s=0} = \mathbf{X_0}$ and $\partial\mathbf{X}/\partial s|_{s=0} = (0, 1, 0)$ at the clamp, while enforcing $\partial^3\mathbf{X}/\partial s^3|_{s=h} = \partial^2\mathbf{X}/\partial s^2|_{s=h} = \mathbf{0}$ and $T|_{s=h} = 0$ at the free end. Equations (S3,S4) are solved following an approach similar to that of Huang *et al.* [7], but the bending term is treated implicitly to allow for a larger time step [6]. The resulting linear system is solved with the *dgesv* routine of *LAPACK*.

Finally, we couple the fluid and the structure at their interface through a no-slip boundary condition, $\dot{\mathbf{X}} = \mathbf{u}[\mathbf{X}(s, t), t]$, guaranteed applying the force distribution computed with a Lagrangian immersed boundary method [6–8]. Our solver is the same previously employed by Monti *et al.* [9], who validated the motion of a single flexible fiber against the analytical predictions reported by Huang *et al.* [7] and the mean flow quantities above and between a rigid canopy against the experiments of Yoshihiko *et al.* [10].

---

* Currently at United College of Engineering and Research, Allahabad, 211010, Uttar Pradesh, India.
† Currently at Universidad Carlos III de Madrid, Leganés, 28911, Madrid, Spain.
‡ E-mail for correspondence: marco.rosti@oist.jp

II. SETUP

Our simulations are carried out in a rectangular volume bounded from above and below by two flat walls extending along the streamwise (x) and spanwise (z) directions. Starting from a domain of size $2.5H \times 2H \times H$ (in x, y and z, respectively) homogeneously discretised over $192 \times 160 \times 96$ points, we later moved to a larger one (Fig. S1a) of size $5H \times 2H \times 2H$ for which we considered two homogeneous discretisations made of $500 \times 200 \times 200$ and $1000 \times 400 \times 400$ points. All grids yielded consistent results for the dynamics of most fibres, but for the few most rigid ones. Given the long computational times needed for the convergence of the statistics associated to the most flexible fibres, we therefore opted for the intermediate resolution introduced above, complementing the outcome with shorter high-resolution simulations for the most rigid fibres. Imposing a fixed flow rate so that $Re = U_b 2H/\nu = 5600$, we confirm that the size of our domain is larger than the minimum one needed to sustain turbulence in numerical simulations [11]. After testing both lower and higher values, we ran all of our simulations at $\Delta t = 1e^{-5} H/U_b$. This time-step proves appropriate to correctly resolve the fastest dynamics of the fibers and of the flow, resulting in a Courant number of $\mathcal{O}(1e^{-3})$ on the finest grid.

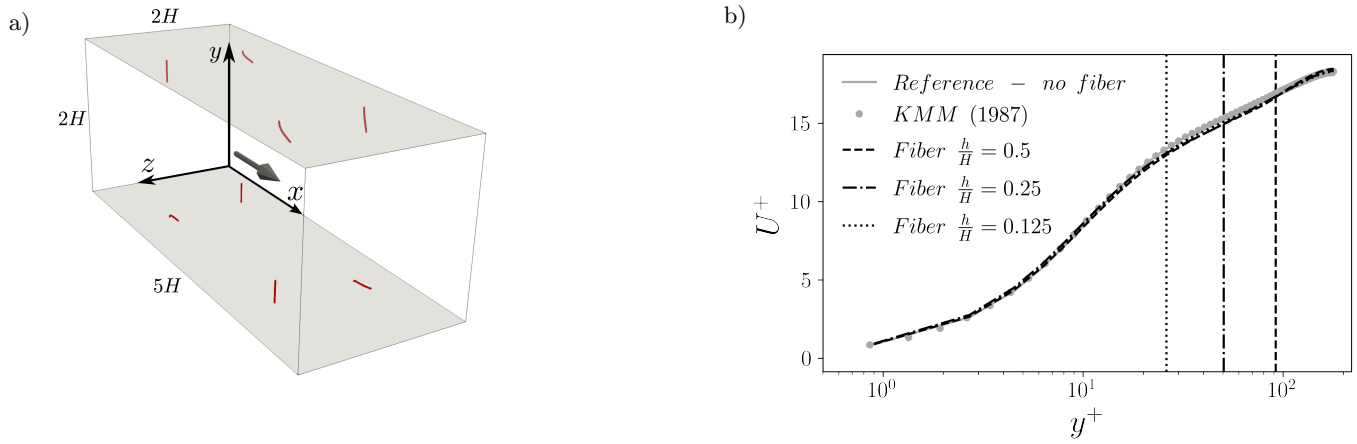

FIG. S1: Panel a reports a sketch of the computational domain adopted throughout our simulations, populated with the fibers of case 3 in table S1. A gray arrow denotes the flow direction. In panel b we show the mean velocity profiles in wall units from our simulations, interpolated at the centre of each grid cell (case 2 from table S1 is omitted, since it yields an outcome which is identical to that of case 1); a reference simulation without fibers is also included. Results are compared to the data of Kim *et al.* [12] in order to asses the adequacy of our numerical setup. Vertical lines mark the vertical coordinate corresponding to the fiber length h of the different cases.

The channel is populated with flexible fibers of different rigidities, vertically clamped at the upper and lower walls and protruding towards the centreline (Fig. S1a). We consider logarithmically distributed values of the Ca down to a minimum dictated by the capability of our code to resolve the motion of the most rigid fibers. Simulations are repeated for different fiber lengths (h) and density ratios between fiber and fluid (ρ_s/ρ_f), thus spanning the parameter space reported in table S1. After assessing the independence of the fibre motion from the number of Lagrangian points, we choose it as in table S1, to have a Lagrangian grid spacing comparable to the Eulerian one.

Since the purpose of our study is to investigate the dynamics of a single flexible fiber in wall turbulence, rather than that of an hairy surface, we must ensure that the fibers contained in the computational domain are sufficiently far from each other not to affect the mean flow significantly, and therefore behave as independent entities. We verify this in Fig. S1b, by comparing the mean velocity profiles from our simulations to those reported by Kim *et al.* [12] for a turbulent channel flow at the same Reynolds number. All the curves shown in the figure exhibit a good agreement, thus validating our numerical setup.

TABLE S1: Parameter space investigated with our simulations.

Case	h/H	ρ_s/ρ_f	$Ca_{min} \backslash Ca_{max}$	# Lagrangian points
1	0.5	1.08	$2.5 \times 10^{-2} \backslash 2.5 \times 10^{5}$	40
2	0.5	1.8	$2.5 \times 10^{-2} \backslash 2.5 \times 10^{4}$	40
3	0.25	1.08	$3.1 \times 10^{-3} \backslash 3.1 \times 10^{3}$	20
4	0.125	1.08	$3.9 \times 10^{-4} \backslash 3.9 \times 10^{-1}$	10

III. TIME HISTORIES

Here we observe the time evolution of the spanwise tip position for five fibers of decreasing rigidity, two laying in the $f_{flap} \approx f_{nat}$ regime, one in the $f_{flap} \approx f_{nat} \approx f_{turb}$ regime, and two in the $f_{flap} \approx f_{turb}$ regime of the map in Fig. 6. Only ten bulk time instants are considered for the purpose of this plot, even thought our simulations were run for much longer: we sampled the fiber position and velocity every $\tilde{\Delta}t = 1e^{-3}H/U_b$ over a total time of $300H/U_b$ for the more flexible fibers (characterised by a slower dynamics) and $100U_b/H$ for the more rigid ones (characterised by a faster dynamics), excluding the initial transients. The two more rigid fibers in Fig. S2 oscillate at their natural frequencies with a nearly-sinusoidal motion, consistently with the bimodal PFD in Fig. 3b. The two more flexible ones, instead, sway with a time scale of $\mathcal{O}(H/U_b)$. In general, the lateral oscillation amplitude of the fibers grows for increasing values of Ca (Fig. 2b). Nevertheless, we also observe a further moderate increase in the intermediate regime where $f_{flap} \approx f_{nat} \approx f_{turb}$, suggesting a resonance effect. This behaviour appears consistent with the elastic energy peak noticed by Rosti *et al.* [1] for intermediate values of the rigidity.

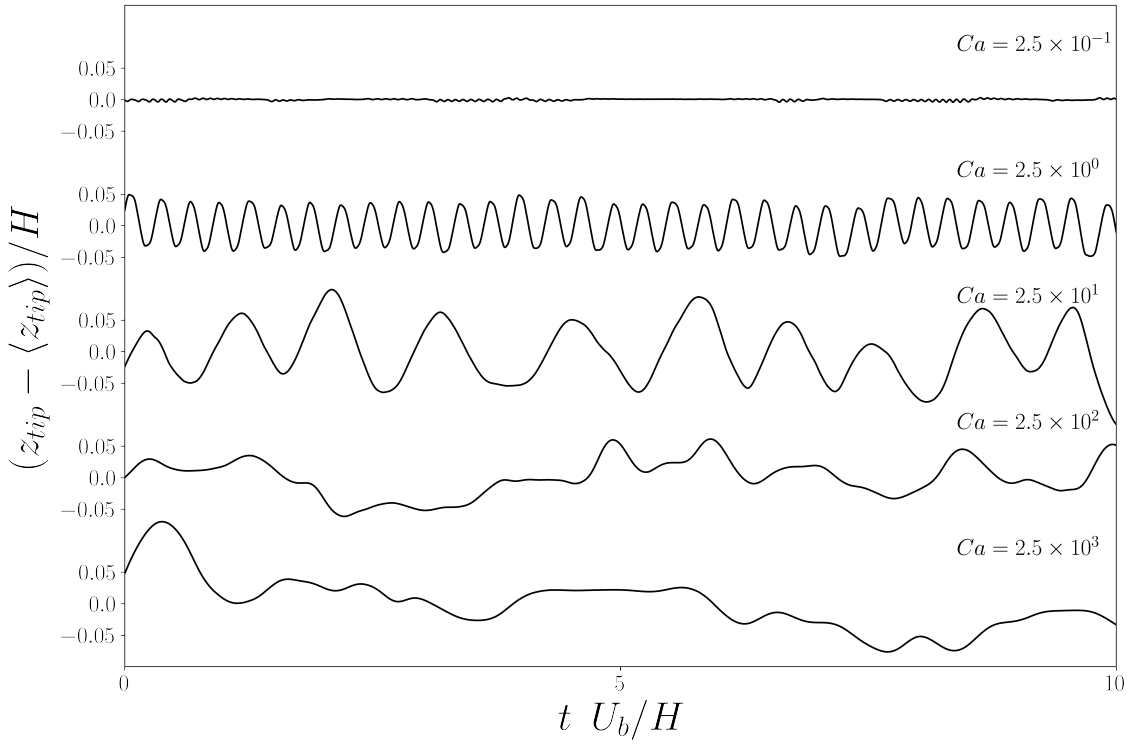

FIG. S2: Spanwise position of the tip of five fibers from case 1 of table S1, for increasing values of Ca. The lateral oscillation amplitude of the fiber with $Ca = 2.5 \cdot 10^1$ (for which $f_{flap} \approx f_{nat} \approx f_{turb}$) appears larger than that of its neighbors, suggesting a resonance effect.

IV. HIGH-FREQUENCY SCALING OF THE TEMPORAL SPECTRA

After reaching their respective maxima at a frequency close to f_{turb} or f_{nat}, respectively, the temporal spectra of the spanwise fiber tip velocity shown in Fig. 4 of the main text are characterised by a decay $f^{-2+\xi}$ that we claim to depend on the forcing seen by the fiber in the flow region it spans during its motion, consistently with the arguments of Jin *et al.* [13]. In particular, the more flexible fiber is deflected in the lower part of the viscous wall region and it is forced by a smooth turbulent field, determining the $\xi \approx -3$ scaling of the Lagrangian spectrum, while the more rigid one extends in the buffer layer, recovering $\xi \approx -5/3$. To support these statements, we compute the temporal spectra of the turbulent kinetic energy (E) at the wall distances corresponding to the mean positions of the deflected fiber tips. As visible in panel *a* of Fig. S3, the Eulerian spectrum at the position corresponding to the fiber with $Ca = 3.1$ tends towards $f^{-5/3}$, while that at $Ca = 3.1 \cdot 10^2$ exhibits a steeper decay. We impute the sharper trends observed in the case of the Lagrangian spectra to the integral effect exerted by the fiber on the high frequency fluctuations.

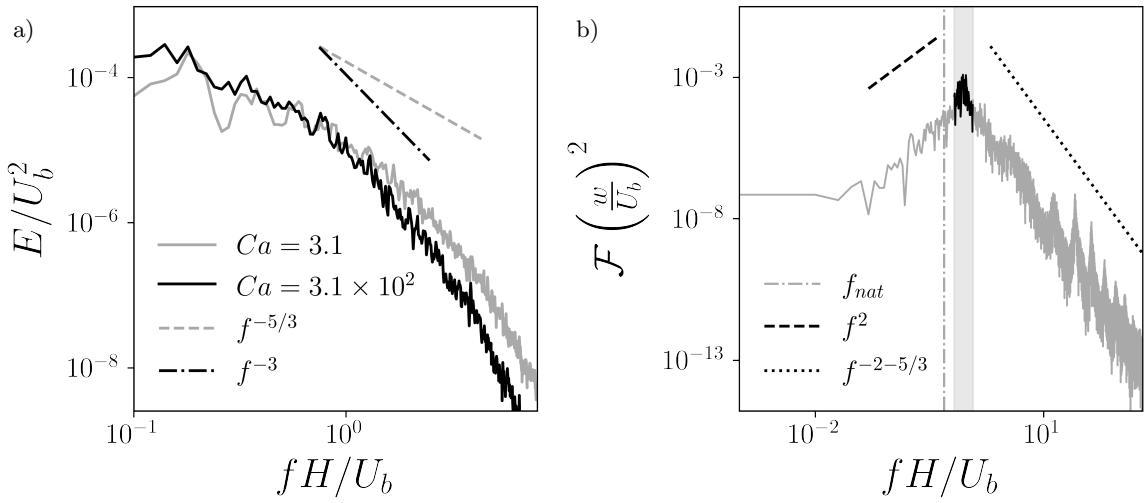

FIG. S3: Further details on the high-frequency scaling of the temporal spectra. In panel a we report the Eulerian temporal spectra of the turbulent kinetic energy (E) at a wall distance corresponding to the mean deflected tip positions of a more rigid ($Ca = 3.1$, $h = 0.25H$, $\rho_s = 1.08\rho_f$) and a more flexible ($Ca = 3.1 \cdot 10^2$, $h = 0.25H$, $\rho_s = 1.08\rho_f$) fiber. The former tends towards $f^{-5/3}$, while the latter exhibits a sharper decay compatible with f^{-3}. Panel b shows the Lagrangian temporal spectrum of the fiber tip spanwise velocity for a fiber ($Ca = 25$, $h = 0.5H$, $\rho_s = 1.08\rho_f$) clamped vertically at $y/H = 0.075$, in the middle of the flow. While the fiber is oscillating at the turbulent frequency dictated by the flow, a $\xi \approx -5/3$ decay is observed, thus confirming the independence of the scaling from the regime of oscillation of the fiber.

Furthermore, we prove that the slope of the high frequency region of the spectra is independent from the regime of motion of the fiber. By clamping vertically one of the fibers with intermediate flexibility of case 1 (see table S1) in the middle of the flow, at a distance from the wall of $y/H = 0.075$, its tip lays well within the buffer layer. A $\xi \approx -5/3$ decay is observed in this case for the temporal spectrum of the spanwise fiber tip velocity, even if the fiber is swaying at the turbulent frequency dictated by the flow and not at its natural one, f_{nat}. The Lagrangian spectrum reported in panel b of Fig. S3 therefore confirms that the high frequency region is dominated by the forcing to which the fiber is exposed.

[1] M. E. Rosti, A. A. Banaei, L. Brandt, and A. Mazzino, Flexible Fiber Reveals the Two-Point Statistical Properties of Turbulence, Phys. Rev. Lett. **121**, 044501 (2018).
[2] A. Mazzino and M. E. Rosti, Unraveling the Secrets of Turbulence in a Fluid Puff, Phys. Rev. Lett. **127**, 094501 (2021).
[3] J. Kim and P. Moin, Application of a fractional-step method to incompressible Navier-Stokes equations, J. Comput. Phys. **59**, 308 (1985).
[4] F. W. Dorr, The Direct Solution of the Discrete Poisson Equation on a Rectangle, SIAM Rev. **12**, 248 (1970), 2029223.
[5] Z. Yu, A DLM/FD method for fluid/flexible-body interactions, J. Comput. Phys. **207**, 1 (2005).
[6] A. A. Banaei, M. E. Rosti, and L. Brandt, Numerical study of filament suspensions at finite inertia, J. Fluid Mech. **882**, A5 (2020).
[7] W. X. Huang, S. J. Shin, and H. J. Sung, Simulation of flexible filaments in a uniform flow by the immersed boundary method, J. Comput. Phys. **226**, 2206 (2007).
[8] C. S. Peskin, The immersed boundary method, Acta Numer. **11**, 479 (2002).
[9] A. Monti, S. Olivieri, and M. E. Rosti, Collective dynamics of dense hairy surfaces in turbulent flow, Sci. Rep. **13**, 5184 (2023).
[10] S. Yoshihiko, T. Tetsuro, N. Hirotsugu, and K. Tadanori, Experimental study on flow over rigid vegetation simulated by cylinders with equi-spacing., Doboku Gakkai Ronbunshu , 31 (1991).
[11] J. Jiménez and P. Moin, The minimal flow unit in near-wall turbulence, J. Fluid Mech. **225**, 213 (1991).
[12] J. Kim, P. Moin, and R. Moser, Turbulence statistics in fully developed channel flow at low Reynolds number, J. Fluid Mech. **177**, 133 (1987).
[13] Y. Jin, S. Ji, and L. P. Chamorro, Spectral energy cascade of body rotations and oscillations under turbulence, Phys. Rev. E **94**, 063105 (2016).